OPTIMIZED SOLID LIPID NANOPARTICLES FOR ENHANCED ORAL BIOAVAILABILITY AND OSTEOGENIC EFFECT OF IPRIFLAVONE: FORMULATION, CHARACTERIZATION, AND *IN VITRO* EVALUATION

ANISH JOHN [ID], ANOOP NARAYANAN V.* [ID], SUMUKH P. R. [ID], SNEH PRIYA [ID], CHAITHRA RAVIRAJ [ID], HARSHA ASHTEKAR [ID]

Department of Pharmaceutics, Nitte (Deemed to be University), NGSM Institute of Pharmaceutical Sciences Deralakatte, Karnataka-575018, India
*Corresponding author: Anoop Narayanan V.; *Email: anishjohn@nitte.edu.in

ABSTRACT

Objective: This study aimed to enhance the oral bioavailability of Ipriflavone (IP) and evaluate its osteogenic effect on human osteosarcoma cells (MG-63) by developing Ipriflavone-loaded Solid Lipid Nanoparticles (IP-SLN).

Methods: IP-SLNs were prepared using a modified solvent evaporation method with probe sonication. Formulation optimization employed Central Composite Design (CCD) with independent variables, including lipid amount, surfactant concentration, and sonication time. Characterization was performed using Transmission Electron Microscopy (TEM). *In vitro* drug release and ex vivo permeation studies were conducted to assess drug release kinetics and bioavailability. Cytotoxicity, Alkaline Phosphatase (ALP) activity, and calcium deposition studies on MG-63 cells evaluated osteogenic effects.

Results: TEM images showed round particles with an average diameter of 43.24±3 nm, a zeta potential of-9.53 mV, and a drug entrapment efficiency of 76.53±1.84%. *In vitro* drug release from IP-SLN was 79.02% compared to 14.21% from IP after 48 h, following the Korsmeyer-Peppas model and first-order kinetics. Ex vivo permeation of IP-SLN was approximately 2-fold higher than IP dispersion. Cytotoxicity studies revealed no toxicity on MG-63 cells. ALP activity and calcium deposition studies indicated that IP-SLN stimulated osteoblast differentiation, increasing alkaline phosphatase activity and mineralization. Pharmacokinetic studies demonstrated that IP-SLN increased the relative bioavailability by 515% compared to ipriflavone.

Conclusion: IP-SLN formulations significantly improved the oral bioavailability and osteogenic effects of ipriflavone on MG-63 cells, suggesting potential for novel therapeutic applications in osteoporosis treatment.

Keywords: Ipriflavone, Solid lipid nanoparticles, Osteoporosis, Bioavailability

INTRODUCTION

Ipriflavone, a semi-synthetic isoflavone compound, is used as a nutraceutical for treating postmenopausal osteoporosis. As a phytoestrogen, it inhibits bone resorption, maintains bone health by increasing density, and helps prevent osteoporosis in postmenopausal women. As a selective estrogen receptor modulator, ipriflavone modulates osteoclast function to facilitate bone remodelling, reduces bone resorption, and promotes osteoblast proliferation for bone mineralization [1] by obstructing the parathyroid gland [2].

The poor solubility of ipriflavone (0.0009 mg/ml at 37 °C) makes it less available for absorption and bioavailable for pharmacological action [3]. Due to its nano-size, the nano lipid carrier system has numerous advantages, including enhanced solubility, improved mucoadhesion, targeted drug delivery, dual-release behaviour, and increased bioavailability [4]. The lipid material in lipid nanoparticles improves their biocompatibility and health properties, making them optimal for *in vivo* delivery with decreased immunogenicity and toxicity [5]. The lipoidal carriers exhibit higher loading capacity for lipophilic drugs and provide protection against enzymatic degradation due to their well-structured crystal lattice [6]. Lipids, including triglycerides, glycerides, fatty acids, steroids, and waxes, are used in the production of SLN, which shares characteristics such as a low melting point, solidity, and body temperature, and is stable concerning several surfactants and co-surfactants, including span, tween, and poloxamer [7]. SLN is effectively encapsulates diverse drugs, including hydrophilic compounds like ampicillin, ascorbic acid, diclofenac sodium, doxorubicin, and insulin, as well as lipophilic drugs such as dexamethasone, melphalan, curcumin, atorvastatin, and naproxen [8, 9].

Numerous administration routes, including parenteral, oral, topical, ocular, inhalation, and nasal, have been investigated for the treatment of tuberculosis [10], cerebral infarction [11], leukaemia [12], and neurodegenerative disorders [13]. Parenteral administration of SLNs is promising for the treatment of maladies such as neoplasia [14], breast and ovarian cancer [15, 16].

Studies have shown that SLN can improve the therapeutic efficiency of the drug by gaining access to the systemic circulation via lymphatic circulation by subclavian and jugular veins. Wei *et al.*, Resveratrol-loaded solid lipid nanoparticles were incorporated into a scaffold to enhance the osteogenic differentiation of Bone marrow-derived Mesenchymal Stem Cell (BMSC) and facilitate effective bone regeneration [17].

Fundaro *et al.* investigated doxorubicin-loaded stearic acid solid lipid nanoparticles stabilized with PEG 2000 to lower the absorption by Reticuloendothelial System (RES) organs such as spleen and liver, improving lung and brain drug bioavailability in the lung and brain [18].

Ahmad *et al.* developed SLN containing quercetin to inhibit bone loss in osteopenic rats, offering a potential preventive strategy for post-menopausal osteoporosis by inhibiting the expression of rank ligands, which promotes osteoclast differentiation [19].

Developing composite definition approaches makes it possible to improve bioavailability, and this growing area has proven promising. To circumvent ipriflavone's limitations, we propose encapsulating the medicine with SLN to increase its oral bioavailability for better treatment of osteoporosis.

MATERIALS AND METHODS

Ipriflavone (IP) was acquired from Triveni Fine Chemicals (Gujarat, India). Glyceryl Monostearate (GMS) and Span 80 were secured from

LOBA ChemiePvt. Ltd, (Mumbai, India). MEM Eagle's medium for culturing MG-63 cells was procured from Himedia laboratories (Thane, India). Alizarin red dye, p-nitrophenyl phosphate and glutaraldehyde were obtained from LOBA ChemiePvt. Ltd, (Mumbai, India). Lysis buffer, Fetal Bovine Serum (FBS) and sterile phosphate buffer saline pH 7.0 were purchased from Himedia laboratories (Thane, India). Trypsin-EDTA (0.05%), and trypan blue solution (0.4%) were purchased from Gibco (New York, USA). Methanol was 99.5% extra pure and purchased from LOBA ChemiePvt. Ltd, (Mumbai, India).

Selection of lipid by solubility method

The solubility of IP is assessed in lipids such as Glyceryl Monostearate, Stearic Acid, Soya Lecithin, and Cetyl Palmitate. 5 mg of each lipid was added to a 50 ml beaker for each lipid and heated to 80 °C. Subsequently, 100 mg of IP was introduced to the molten lipid and mixed using a water bath shaker. Solubility evaluation relied on visual examination, ensuring the formation of a clear solution without observable drug crystals. This method aids in selecting the most appropriate lipid for effective SLN formulation [20].

Optimization of the ipriflavone SLN by CCD design

For the optimization of Ipriflavone-loaded solid lipid nanoparticle (IP-SLN), a Central Composite Design (CCD) employing three factors at two levels was utilized. The study aimed to optimize the independent variables: lipid amount (X1) ranging from 250 to 450 mg, concentration of span 80 (X2) ranging from 0.5% to 1.5% v/v, and sonication time (X3) ranging from 5 to 15 min. The optimization process was conducted using Design Expert software®. Particle size (in nano meter) (Y1) and Polydispersity Index (PDI) (Y2) served as the dependent variables. The design comprised 20 experimental trials, including six replicates at the centre points to estimate the error in the response results table 1. Formulation selection was based on achieving low particle size and PDI values, and a statistical analysis evaluated the impact of independent variables (X1, X2, X3) on responses (Y1, Y2) [21].

Table 1: Designed formulation parameters and measured responses using central composite design for SLN preparation

Std	Factor A	Factor B	Factor C	Response 1	Response 2
	GMS (mg)	Span 80 (% v/v)	Sonication time (min)	Particle size (nm)	PDI
1	250	0.5	5	41.39	0.407
2	450	0.5	5	49.21	0.471
3	250	1.5	5	57.08	0.475
4	450	1.5	5	40.1	0.454
5	250	0.5	15	63.96	0.477
6	450	0.5	15	53.33	0.428
7	250	1.5	15	75.62	0.536
8	450	1.5	15	48.13	0.581
9	181.821	1	10	61.95	0.477
10	518.179	1	10	41.13	0.419
11	350	0.159104	10	45.17	0.441
12	350	1.8409	10	52.91	0.616
13	350	1	1.59104	36.27	0.367
14	350	1	18.409	53.42	0.398
15	350	1	10	42.67	0.402
16	350	1	10	40.54	0.433
17	350	1	10	41.22	0.442
18	350	1	10	43.74	0.413
19	350	1	10	40.12	0.475
20	350	1	10	44.95	0.484

Formulation of ipriflavone-loaded solid lipid nanoparticle (IP-SLN)

A modified solvent evaporation method was used to formulate IP-SLN. In this method, ipriflavone is dissolved in methanol with surfactant (span 80), and lipid (GMS) at a temperature of 50 °C was added into an aqueous phase containing distilled water was stirred at 900 rpm using a magnetic stirrer. The resultant O/W emulsion was stirred continuously at room temperature for 30 min, followed by probe sonication in optimized condition with 40 % amplitude and 3 seconds on and 2 seconds off pulse conditions in an ice water bath maintained at 20-25 °C. [22-23].

Characterization of ipriflavone-loaded solid lipid nanoparticle

Particle size, polydispersity index and zeta potential

The dynamic light scattering method determined the average particle size and Polydispersity Index analysis of the formulated IP-SLN dispersion using (ZS90, Malvern Zetasizer, UK). The particle size was calculated using the autocorrelation function of the intensity of light scattered from the particles. The Polydispersity Index (PDI) served as a measure of dispersion homogeneity ranging from 0 to 1. The electrophoretic mobility values were obtained with suitable dilutions in water at 25 °C [24, 25].

Morphological determination

Transmission Electron Microscopy (TEM) with bright field imaging and magnification technique was employed to examine the physical characteristics, such as particle size, shape, and surface morphology of IP-SLN [26].

Compatibility study by FTIR

Fourier Transform Infrared (FTIR) spectra were recorded on Bruker FTIR (Germany) in the 4000 cm^{-1}-650 cm^{-1} region to evaluate drug, lipid, and formulation interaction [27].

Entrapment efficiency

The centrifugation technique determined Entrapment Efficiency (EE) by analyzing the amount of free IP in the aqueous phase. The IP-SLN underwent centrifugation in a high-speed cold centrifuge (C 24; Remi India) at 12,000 rpm for 25 min at 10 °C, and the resulting supernatant solution was collected. The quantification of unencapsulated ipriflavone in the supernatant was determined using a UV-visible spectrophotometer (Shimadzu, Japan) at 250 nm. The %EE was calculated as follows.

$$\% \text{ Entrapment Efficiency} = \frac{\text{Total amount of drug added} - \text{free drug in supernatant}}{\text{Total amount of drug added}} \times 100$$

In vitro drug release studies

In this *in vitro* release study, IP-SLN-loaded solid lipid nanoparticles were subjected to analysis using a dissolution Type II test apparatus and a dialysis kit with a pre-soaked 12,000 kDa molecular weight cut-off in pH 6.8 phosphate buffer. A 1 ml aliquot of the IP-SLN nanosuspension was introduced into a dialysis membrane, immersed in 900 ml of pH 6.8 phosphate buffer dissolution medium, with the paddle rotating at 50 rpm, and the temperature maintained at 37 °C ±1 °C in an incubator. At predetermined time intervals (0.25, 0.5, 1, 2, 3, 4, 6, 8 and 24 h), 1 ml of the buffer was withdrawn and

replaced with an equivalent fresh buffer. The amount of released drug was analyzed using the UV method at 250 nm [28].

Ex-vivo permeation studies by sac method

The non-everted gut sac method was employed to evaluate the permeation of IP-SLN across the intestine. The studies were conducted as per the ARRIVE guideline. In this study, White Leghorn Chicks (weighing 800 to 1000g) (n=3) were sacrificed by cervical dislocation technique, and an ileum of 6 cm^{2}was isolated and flushed with a physiological salt solution of pH 7.0 (Krebs-Ringer solution) to remove the luminal contents and mucosal layer. One end of the sac was tied with thread and filled with the optimized 2 ml of IP-SLN nanosuspension (concentration of 12 mg/ml), and the other end was tied. The ileum bag was immersed in 200 ml phosphate buffer with a pH of 6.8. At regular intervals (1, 2, 3, 4, 5 and 6 h), samples were withdrawn from the beaker and analyzed for drug content. The ileum was then sectioned into equal lengths of 6.9 cm each. After flushing the segments with normal saline, they were immersed in phosphate buffer with a pH of 6.8 [29].

In vitro cell-lines studies of IP-SLN

Cytotoxicity studies

MG-63 osteosarcoma cells (Purchased from NCCS, Pune) were cultured in Eagle's Minimum Essential Media with 15% Fetal Bovine Serum and 1% Antibiotic-antimycotic solution at 37 °C, 5% CO2, and 95% humidity. Seeded at 5×104 cells/well in 96-well plates, they were treated with 1% drug (in DMSO and media) and IP-SLN at concentrations from 12.5 to 800 mg/ml. After a 48 h incubation, MTT solution (5 mg/ml, 50 μl**) was added, followed by a 4 h incubation, and then DMSO (200 μl**) to dissolve formazan crystals. Absorbance at 570 nm was measured using a Thermo Scientific microplate reader after purple colour development [30].

Alkaline phosphatase (ALP) activity

Cells were seeded at 1×10^5 cells/well density into a 24-well tissue-culture plate, incubated for 48 h and treated with drug and IP-SLN (concentration 50 μg/ml) in culture media for 24 h. The cells were washed with PBS and then disrupted using 100μl* of cell lysis buffer at intervals of 7, 14 and 21 days. Remove the cell debris by centrifuging at 3,000 rpm at 4 °C for 3 min. The supernatant was incubated with 100μl* of 1% p-nitrophenyl phosphate buffer solution for 30 min at 37 °C. ALP activity was determined by measuring the conversion of p-nitrophenyl phosphate to p-nitrophenol at an optical density of 405 nm using a microplate reader [31].

Determination of calcium mineralization

A total of 1×10^5 cells/well were seeded into 12 well plates and maintained in culture media for 48 h in a 5% CO$_2$ incubator at 37 °C. IP and IPSLN (equivalent to 50 μg/ml) were added into the wells, and cells were incubated. The cells were stained with a 2% alizarin red dye solution of pH 4.2 for 45 min. Free unbound Alizarin Red Stain (ARS) dye from cells was removed by washing with PBS and detected using Magnus Magcam HD pro digital camera through a light microscope at 10x magnification [32].

Cell extracellular matrix stained by the alizarin red dye was extracted for calcium deposit quantification using 10% acetic acid. 800 μl** of acetic acid was added to each well, and the plate was incubated at room temperature with shaking for 2h. Then 200 μl** of 10 %v/v ammonium hydroxide was added to neutralize the acid.

Sometimes, pH was measured at this point to ensure it was between 4.1 and 4.5. Aliquots (150 μl**) of each well in triplicates were transferred to 96 well plates and read at 405 nm using a multimode microplate reader [33].

Pharmacokinetic studies

Animals and blood collection

Male Wistar rats weighing 250-300 g were used in the study. The pharmacokinetic study protocol was approved by the institutional Animal Ethical Committee, NITTE (DU) (Approval number is NGSMIPS/IAEC/AUG-2023/369), Mangalore. Three groups (control, IP and IP-SLN) containing 6 animals were used for the study. Three animals were housed in cages, with free access to water 12 h before the study. The pure ipriflavone and the optimized IPSLN were administered orally at 50 mg/Kg doses. 200 μl of blood were collected using heparinized capillaries from the retro-orbital plexus in the time interval of 0,5,15,30,60,120,180 and 240 min. The blood samples were centrifuged at 10,000 rpm for 5 min. The plasma was separated and stored at-80 °C until further analysis. The samples were analysed using the HPLC method.

Extraction and analysis in plasma

Approximately 100 μl of plasma was taken in the 1.5 ml centrifuge tube and the supernatant after centrifugation at 10000 rpm for 5 min. Then 100 μl of HPLC grade solvent acetonitrile was added to precipitate the proteins. Centrifuge the samples again with the same conditions above and transfer the clear supernatant to the HPLC vial, and 40 μl** was injected into the HPLC system for analysis.

The pharmacokinetic parameters such as Area Under the Curve (AUC), terminal elimination rate constant (β), Clearance (Cl), Volume of distribution (Vd), half-life (t½), Cmax and Tmax are calculated using PK solver software [34].

Statistical analysis

Statistical analysis was carried out, and ANOVA analysed the difference in the parameters at 95% confidence interval. The difference was considered statistically significant at $p<0.05$.

Short-term stability studies

The stability study of the prepared SLN was conducted as per ICH guidelines at controlled temperature and humidity, i. e., 4±2 °C/35±% RH, 15±2 °C/45±2 % RH and 25±2 °C/60 % RH for three months. The stability was measured in terms of physical appearance, particle size, and zeta potential, and PDI was observed in specific periods: 0, 1, and 3 mo.

RESULTS AND DISCUSSION

Solubility of Ipriflavone in lipid

The solubilizing power of lipids with the drug is crucial in preparing SLN. The lipid more capable of solubilizing the IP was selected by observing the turbidity. The high drug solubility in lipids can increase entrapment efficiency and drug loading [35]. Low drug lipid solubility may also prevent drug molecules from linking to the lipid, leaving the drug free and failing to give the intended controlled release. From table 2, it was concluded that the GMS can solubilize a higher amount of IP when compared to other lipids by observing the transparency. This may be due to mono-, di and triglycerides. Long-chain fatty acids attached to the glyceride and less ordered crystal lattice resulted in increased accommodation of IP [36].

Table 2: The solubility analysis of ipriflavone in various lipids

Drug	Lipids	Appearance of solution after adding drug
Ipriflavone	Glyceryl monostearate	Transparent
	Stearic acid	Slightly turbid
	Cetyl palmitate	Turbid

Optimization of IP-SLNs

CCD was found to be very effective in considering the effects of independent formulation variables to develop an optimized IP-SLN

formulation consisting of GMS (Lipid), Surfactants (Span 80) and Ipriflavone (Drug) primarily prepared using a modified solvent evaporation method. The optimized formulation composition consists of 271 mg of GMS, 1 % v/v of span 80 and a sonication time

of 5 min. The particle size of the selected experiment run was 41.48 nm, and the PDI value was observed to be 0.394.

Influence of factors on particle size (Y₁)

The impact of factors such as concentration of GMS span 80 and sonication time were assessed on the particle size by the 3D response surface shown in 1. The plots and equation obtained using the significant model terms showed that particle size decreased with increased GMS concentration. The inverse relationship between particle size and GMS concentration suggests that GMS functions as an emulsifier, promoting the stability of the lipid emulsion during SLN formation along with the span 80. Higher GMS concentrations facilitate more significant interfacial tension reduction between the lipid and aqueous phases, thereby enhancing the emulsification process and resulting in smaller lipid particles and, subsequently, smaller SLN particle sizes [37]. The positive coefficient of factor C (sonication time) inversely affects the particle size. Analysis of 1 shows that prolonged

sonication increases particle size, indicating that too much sonication causes particles to aggregate rather than break down. Sonication increases particle velocity, leading to more frequent collisions. However, if the particles lack sufficient zeta potential, they may not be able to repel each other effectively, causing them to aggregate upon contact instead of dispersing [38]. The quadratic coefficient studied affects the span 80 on particle size. At low concentrations of surfactants, complete coverage of nanoparticles occurs [39]. As the concentration of Span 80 increases up to 1%, interfacial tension reduction between the interphase ensues, forming smaller particles and inhibiting coalescence. However, exceeding a 1% concentration of Span 80 accumulates multiple surfactant layers on the particle. The lipoidal properties of Span 80 also contribute to the increase in particle size [22]. Span 80 adsorbs onto the particle surface, neutralizing or diminishing electrostatic repulsion between particles. Decreased repulsive forces facilitate particle contact and aggregation, resulting in larger particle sizes.
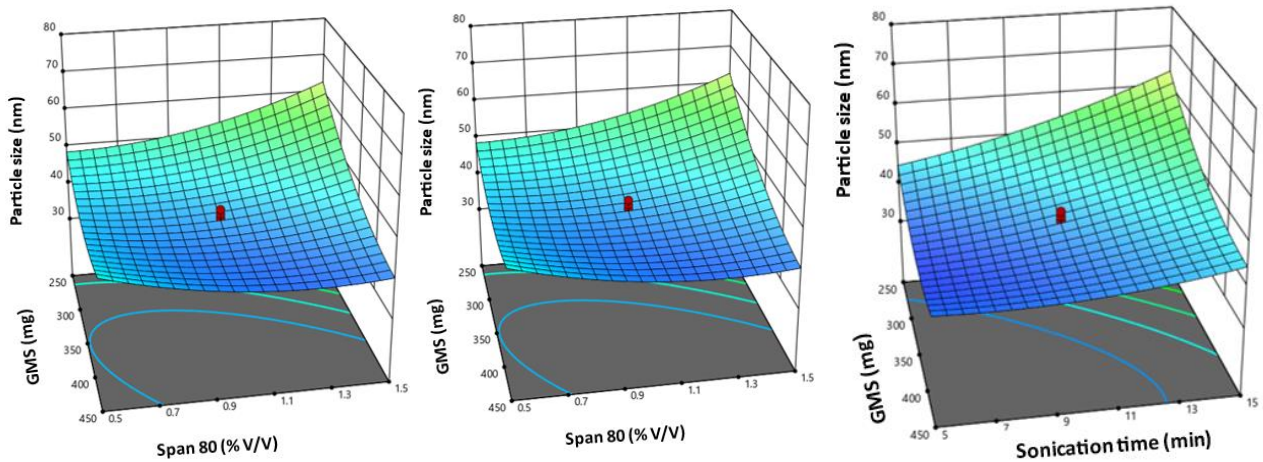

Fig. 1: Response surface plot of independent variables GMS, Span 80, and sonication time on particle size

Influence of factors on PDI (Y₂)

The influence of all the three investigated factors, GMS, span 80, and sonication time (X_1, X_2, X_3) on PDI (Y_2) has been depicted in the 3D response surface plot in 2. PDI analysis showed that the lipid concentration and sonication time do not significantly impact

the Particle size distribution of SLN. The concentration of surfactant has a significant impact on the PDI. PDI increases as the span 80 concentration increases due to its non-ionic nature that neutralizes the repulsion forces between the particles and leads to the enlargement of the formed aggregates, thus increasing PDI [40].
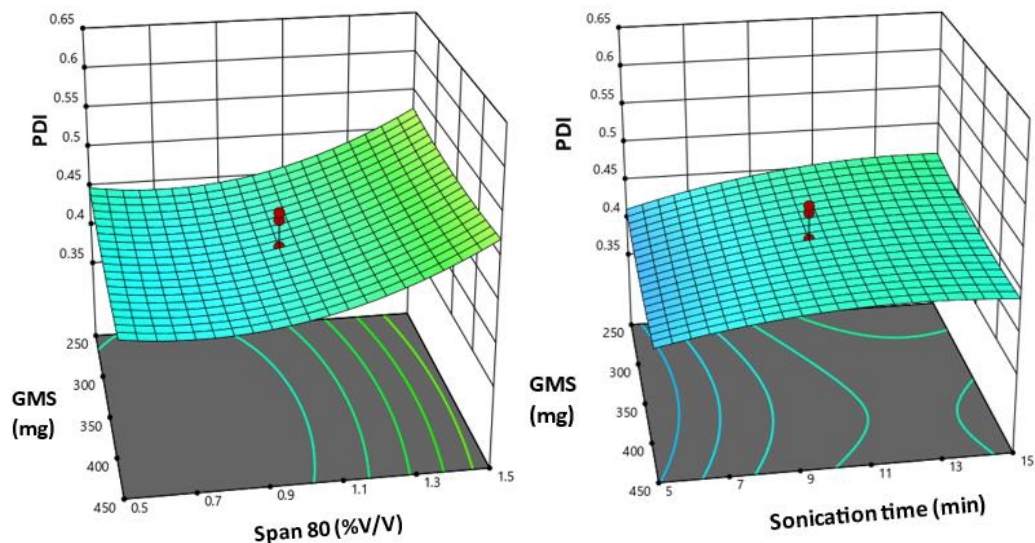

Fig. 2: Response surface plot of independent variables GMS, Span 80, and sonication time on PDI

Formulation of IP-SLNs

The excipients and concentrations for preparing IP-SLN were selected considering the physicochemical properties and CCD optimization technique. The ipriflavone is combined with lipid by a solvent evaporation method followed by probe sonication at the amplitude of 40% for 5 min. The appropriate selection of lipids, surfactants and processing parameters can produce nano-size particles.

Characterization of IP-SLN

Average particle size, polydispersity index and zeta potential

The formulation prepared by the ultra-probe sonication method showed a size range of 43.24±3 nm. Smaller particle sizes contributed majorly to the amount of GMS in the formulation. As GMS is a lipid, it shows the property of an emulsifier as well. The formulation is then stabilized by the span 80, preventing the dispersed particle's agglomeration in the nano-suspension [41]. The PDI of IP-SLN was found to be 0.396, indicating that prepared lipid nanoparticles have a relatively uniform size. The Zeta potential of the IP-SLN was determined to be-9.53 mV. The negative sign in the formulation indicates the repulsive forces and the possible reason for negative values corresponds to the presence of fatty acids in GMS, which are released by hydrolysis in SLN. As the zeta potential

is less, there are no sufficient repulsion forces between the particles, leading to the loose aggregation of particles over time. The negative (anionic) charge displays advantageous characteristics for oral particle absorption, including enhanced lymphatic transport and reduced lipolysis. However, cellular uptake is hindered due to repulsion with biomembrane [42].

Morphology analysis

The morphological character of SLN plays an essential role in cellular uptake and internalization of nanoparticles [43]. The TEM image of the SLN reveals essential insights into their morphology and structure 3 shows spherical nanoparticles with a relatively homogeneous size distribution, indicating a successful formulation process. The average particle size of the SLN appears to be around 43 nm, with minimal variation. TEM image suggests that the formulation method employed effectively controlled the particle size. The spherical shape of nanoparticles offers advantages such as enhanced surface area-to-volume ratio, prevention of structural deformations due to the absence of sharp edges, and efficient packing compared to irregularly shaped particles [44]. Spherical nanoparticles tend to follow the streamlines of the flow they are travelling in [45]. Spheres are internalized more quickly by endothelial cells [46].
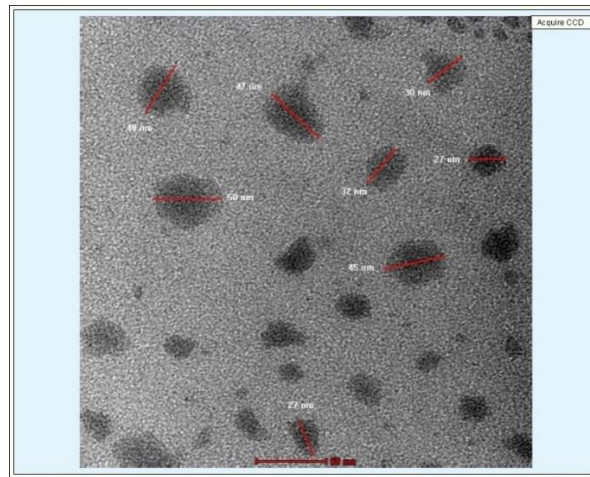

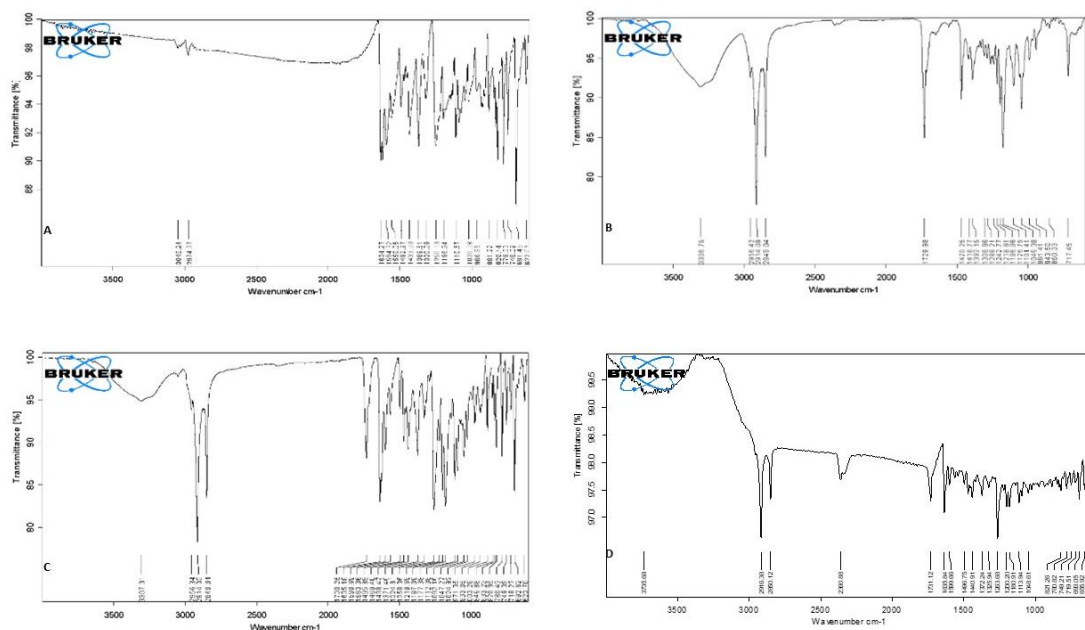**Fig. 3: TEM characterisation of IP-SLN. Scale bar: 50 nm**

Fig. 4: FT-IR spectra of A. Ipriflavone, B. GMS, C. IP with GMS, D. IP-SLN

FTIR analysis

The FTIR spectra of IP, GMS, IP+GMS physical mixture and IP-SLN are presented in 4. Loading IP into the SLN nanoparticles still shows the characteristic absorption peaks of IP at 1634 (C=O), 1433 (C-O-H), 1250 (C-O), and 748 (C-H) cm^{-1} in the corresponding positions of IP+GMS and IP-SLN. Comparing the spectra of GMS with IP+GMS and IP-SLN nanoparticles shows that the prominent absorption peaks of GMS at 3311 (O-H), 2917 (CH$_3$stretch), 2850 (CH$_2$ stretch), and 1732 (C=O) cm^{-1} appeared in the IP+GMS and IP-SLN nanoparticle spectra. FT-IR interpretation revealed that all the excipients used were compatible with ipriflavone, and there were no signs of interactions between the drug and the excipients used.

Entrapment efficiency

The entrapped efficiency of the ipriflavone in the optimized formulation is determined to be 76.53±1.84%. This notable entrapped efficiency can be attributed to the favourable solubility of the drug in GMS and its compatibility with other components utilized in the formulation. As ipriflavone exhibits poor solubility in water, the drug remains enclosed within the lipid matrix due to a higher affinity, further enhanced by a surfactant to prevent drug expulsion.

***In vitro* drug release**

The cumulative release of IP from the SLN (79.02%) was significantly higher than from the IP dispersion (14.21%) within 48

h Fig. 5. The nano-size of the SLN provided a large surface area for drug release, facilitating the dissolution of ipriflavone into the medium and promoting drug release.

Kinetic analysis table 3 indicated that drug release from SLN followed first-order kinetics (R^2 = 0.9688). This implies that the drug release rate decreases exponentially over time, suggesting a Fickian diffusion-controlled release mechanism. The R^2 values and release rate constants for each kinetic model were determined. The Korsmeyer-Peppas model, with the highest R^2 value of 0.971, analyses drug release from polymeric nanocarrier system. It suggests that the release of ipriflavone from IP-SLN follows a non-Fickian diffusion mechanism, indicating a combination of diffusion and erosion processes. The Korsmeyer-Peppas model showed an R^2 value above 0.95. These findings suggested that the proposed mechanism of drug release from SLN may be non-Fickian diffusion by swelling, erosion, or relaxation coupled with diffusion. SLN composed of lipids could undergo swelling in the release medium, leading to matrix expansion and the formation of channels for drug release. Matrix erosion or degradation contributed to drug release over time. The size and shape of SLN played a role in non-Fickian release, with the small size allowing for increased surface area-to-volume ratio, faster initial drug release, and sustained release through diffusion within the swollen or eroded matrix. Controlled release prolonged therapeutic effects and reduced drug administration frequency [47].
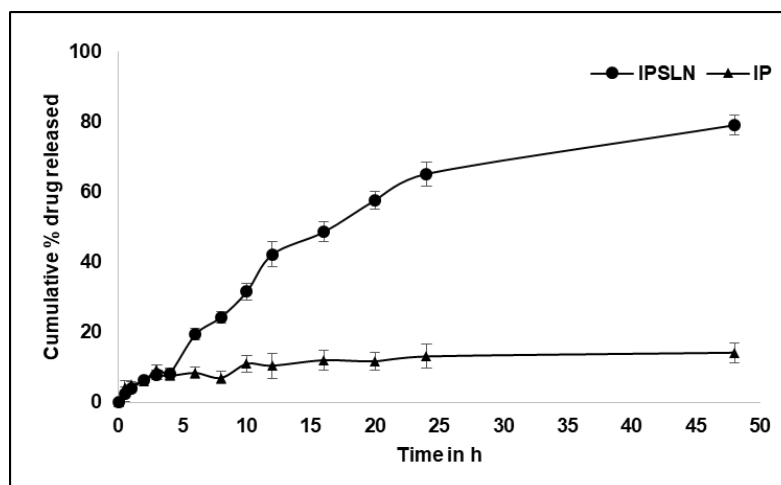

Fig. 5: *In vitro* release from IP-SLN over 48 h in phosphate buffer pH 6.8, and the results are expressed as mean values of three different experiment standard deviations. All data related to IP-SLN is statistically significant with respect to free IP data

Table 3: Kinetic model and the R^2 for predicting the mechanism of drug release from IPSLN

Model	R^{2}value
Zero-order	0.959
First order	0.9688
Higuchi model	0.9262
Korsmeyer-Peppas	0.9711

Ex-vivo permeation study

IP-SLN were subjected to a permeation profile using chicken ileum, and the results in 6 were compared against drug dispersion in a phosphate buffer of pH 6.8. The results of permeation rate across the intestinal ileum region have shown the IP-SLN exhibited a maximum % cumulative amount of drug permeated across the ileum than drug dispersion. Permeation data in this study revealed that the % cumulative amount of drug permeated for IP-SLN was found to be 77.34% after 6.5 h. In the case of drug dispersion, the % cumulative amount of drug permeation was 48.47 %. Thus, IP-SLN showed 1.59-fold higher permeation when compared to drug dispersion. Higher permeation of SLN can be correlated with the lesser particle size, as

the nano-size provides a larger surface area for interaction with the intestinal epithelium. Increased surface area can improve contact and enhance permeation. The lipophilic nature of SLN, which mimic physiological components, facilitates their rapid traversal across the intestinal barrier through easier engulfment via endocytosis [48]. The nano size of SLN enables them to demonstrate bio-adhesive properties, allowing them to adhere to the wall of the gastrointestinal tract or penetrate the inter-villar spaces [49].

***In vitro* cell lines studies**

***In vitro* cytotoxic studies (MTT assay)**

Cell viability of IP-SLN and IP was determined after 24 h exposure to MG-63 cells. The results indicated that the % viability of cells exposed to the drug solution and IP-SLN did not exhibit cytotoxicity at all dilutions. The minimal viability of MG-63 cells was 64.84% and 54.76%, respectively, after 24 h of treatment with 1 mg/ml of IP-SLN and drug. IC50 value, the concentration of substance required for 50% cell death for drug and IP-SLN, was found to be 1.3 mg/ml and 1 mg/ml, respectively. The significant decrease in cellular viability observed with IP-SLN highlights the importance of optimizing the concentration of excipients in the formulation, as these components

may influence cell viability [50]. The therapeutic effectiveness of drug-loaded solid lipid nanoparticles (SLNs) relies on multiple factors, including cellular uptake, intracellular distribution, and the quantity of drug accessible from the internalized SLNs within the cell.
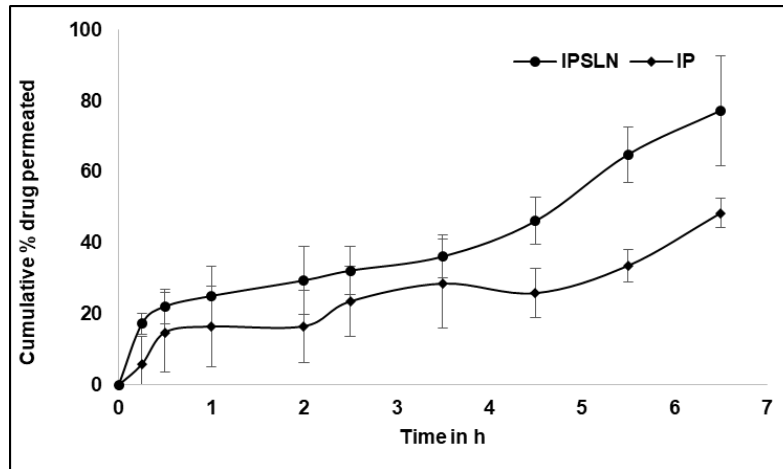

Fig. 6: Ex vivo permeation of IP and IP-SLN through chicken ileum. Error bars indicate SD values of triplicate

Alkaline phosphatase (ALP) activity

ALP activity and calcium deposition are commonly utilized markers to assess the early and late stages of osteoblast differentiation during bone regeneration [51]. ALP activity of MG-63 cells cultured with IP-SLN and control was compared to those of the drug dispersion till 21 days. The investigated substance can induce the differentiation of MG-63 towards the osteoblastic phenotype. Cells treated with the control are considered blank. As shown in 7., ALP activities of MG-63 cells treated with IP-SLN showed a gradual increase throughout 21 days, as the drug must diffuse from the matrix and then undergo dissolution later taken up by the cells. The dissolution of the ipriflavone in Dimethyl Sulfoxide (DMSO) exhibited a prompt enhancement in osteoblast activity due to the absence of any rate-limiting barrier.

Consequently, the drug became readily accessible for uptake by cells. The increase in the activity may be due to drug-induced alterations in intracellular signalling pathways, gene expression patterns, and cellular microenvironments, ultimately impacting ALP activity [52]. The release characteristic of IP-SLN makes the drug available at the site of action for longer, which can be beneficial for prolonged osteoporosis treatment. Our study observed that the ALP activity exhibited a significant and progressive increase over time by treating the cells with IP-SLN, thus indicating that the entrapped ipriflavone was efficiently released within the cells, thereby exerting a positive effect on osteogenesis and providing evidence of simulation of differentiation of osteoblasts [53].

Alizarin red staining detection and quantification of mineralisation

When osteoblasts undergo differentiation, they initiate the mineralization of the bone matrix. The efficacy of Alizarin Red Stain (ARS) in promptly binding to calcium salts makes it a widely used method for assessing calcium accumulation in cells [33]. Mineralization of MG-63 cells treated with IP and IP-SLN was studied for 21 d. The optical microscopic image of cells stained with ARS confirmed mineral deposition in the cells 8. Calcium deposition in MG-63 cells treated with pure drug was found 1.09 folds higher than IP-SLN on the 21st day, as shown in 9. The development of calcium-rich deposits on cell lines treated with samples proved the matrix mineralisation process. This study showed that the IP-SLN can induce mineralization in osteoblast cells, which can treat bone deformities by enhancing the osteoblast cell's activity.
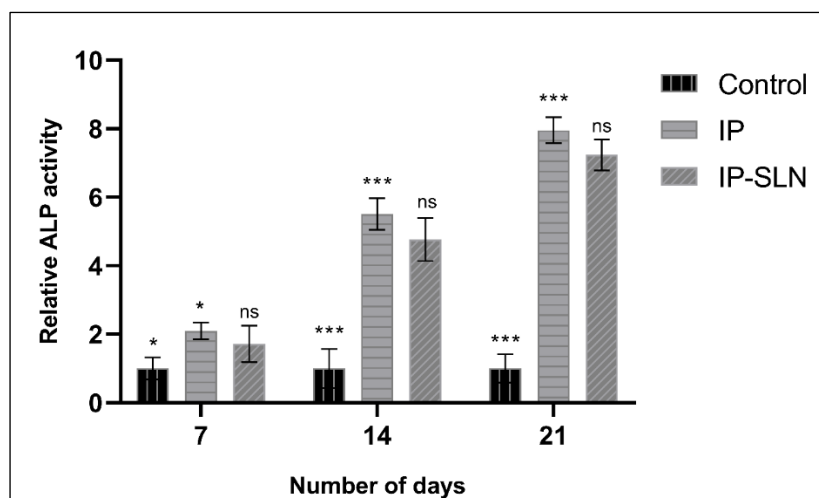

Fig. 7: ALP activity of MG-63 cells treated with ipriflavone and IP-SLN for 21 days. The data is represented in mean±SD, n=3 and analyzed by two-way ANOVA. *$p<0.05$, *<0.0001 and>0.05 is ns**
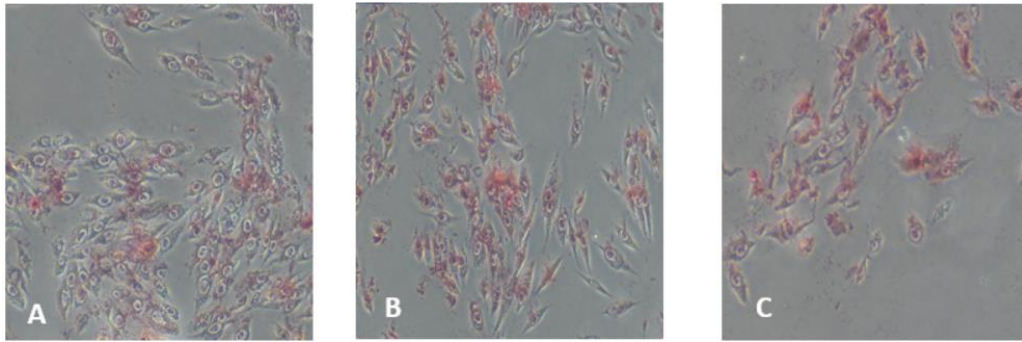
Fig. 8: Mineralization of differentiating MG-63 cells treated with IP-SLN for A) 7, B) 14 and C) 21 d, detected by Alizarin red stain
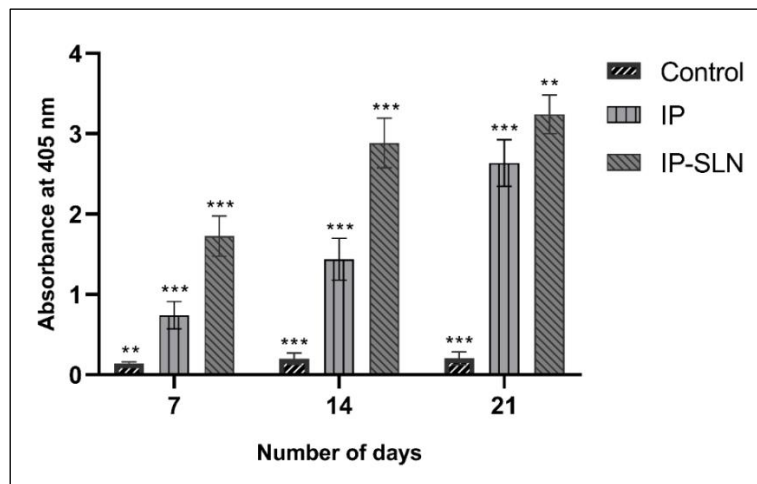

Fig. 9: Calcium deposition of MG-63 cells treated with ipriflavone and IP-SLN for 21 d, detected by alizarin red staining. This data is represented in mean±SD, n=3 and analyzed by two-way ANOVA. *p<0.05, *<0.0001 and>0.05 is ns**
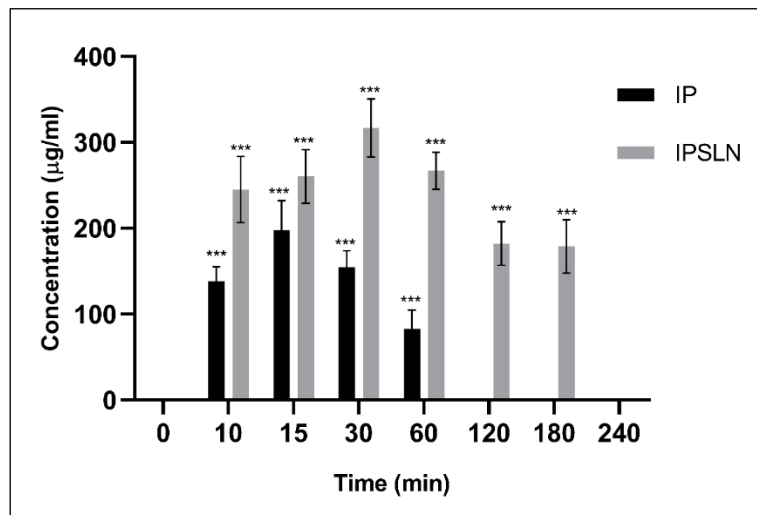

Fig. 10: Plasma concentration profile of ipriflavone and ipriflavone loaded SLN. Data is represented in mean±SD, n=3 and analyzed by two-way ANOVA. *p<0.05, *<0.0001 and>0.05 is ns**

Pharmacokinetic studies

The pharmacokinetic comparison between IP and IP-SLN reveals significant differences in bioavailability and systemic exposure. The pharmacokinetic parameters of IP and IP-SLN are given in table 4. The ipriflavone exhibited a rapid time to reach maximum plasma concentration (Tmax) of 15±2 min, and ipriflavone-loaded SLN demonstrated a delayed Tmax of 30±4 min. This delayed absorption suggests a slower release of ipriflavone from the SLN formulation, likely due to the sustained release properties of the nanoparticles. Regarding maximum plasma concentration (Cmax) and area under the curve (AUC), ipriflavone-loaded SLN showed substantial increases compared to IP. Cmax increased from 197.71±14.5 µg/ml for IP to 316.62±27.9 µg/ml for ipriflavone-loaded SLN, while AUC increased from 12091.16±201.62 µg/ml/min to 84582.87±741.87 µg/ml/min, respectively. This significant enhancement in Cmax and

AUC indicates improved systemic exposure and bioavailability of ipriflavone when formulated as SLN. Despite a shorter half-life (T½) for IP-SLN compared to pure ipriflavone (24.52±3.18 min vs. 35.20±2.36 min), the mean residence time (MRT) was notably higher (266.00±31.02 min vs. 57.23±12.75 min). This suggests a prolonged IP-SLN in the systemic circulation, potentially attributed to sustained release characteristics.

Furthermore, the relative bioavailability of IP-SLN was significantly increased to 515.07±15.87% compared to pure ipriflavone. These findings underscore the potential of SLN as an effective delivery system for enhancing the therapeutic efficacy of ipriflavone, offering prolonged and sustained release for improved patient compliance and therapeutic outcomes. The plasma concentration profile of IP and IPSLN is depicted in 10.

Table 4: Pharmacokinetic paratmerts of ipriflavone and ipriflavone SLN

Parameters	Units	Ipriflavone	Ipriflavone SLN
T_{max}	min	15±2	30±4^
C_{max}	µg/ml	197.71±14.5	316.62±27.9^
AUC (0-α)	µg/mlmin	12091.16±201.62	84582.87±741.87^
T½	min	35.20±2.36	24.52±3.18^
CL	(µg/ml)/min	0.001±0.00	0.0005±0.00^
V_d	µg/ml	0.06±0.001	0.14±0.005^
MRT	min	57.23±12.75	266.00±31.02^
Relative F	%	-	515.07±15.87^

These values are expressed as Mean±SD. **^**Shows a significant difference in parameters at $p<0.05$ as compared to ipriflavone

Short-term stability studies

The prepared IP-SLN was found to be physically stable, with a slight change in particle size, PDI, and zeta potential compared to the initial values for 30 d. The results of the stability study at different temperatures for evaluated parameters of IP-SLN are shown in table 5. A slight change in the responses is seen due to the lesser zeta potential, which causes nanoparticle aggregation during storage. The consistency in formulation parameters across different environmental conditions indicates robustness in the manufacturing process of IP-SLN. This is crucial for ensuring reproducibility and reliability in the performance of the nanoparticles for various applications, such as drug delivery systems. In addition, assessing the long-term stability of the nanoparticles under varying environmental conditions could provide a more comprehensive understanding of their behaviour.

Table 5: Stability studies of IP-SLN

Formulation	Parameter	Temperature C/Humidity (% RH)	Month		
			0	1	3
IP-SLN	Particle size (nm)	4±2/35±2	43.53	43.78	47.45
		15±2/45±2	42.65	43.21	48.31
		25±2/60±2	43.85	43.45	49.78
	PDI	4±2/35±2	0.398	0.412	0.425
		15±2/45±2	0.374	0.386	0.418
		25±2/60±2	0.385	0.399	0.417
	Zeta potential (mV)	4±2/35±2	-9.83	-9.83	-9.93
		15±2/45±2	-9.76	-9.83	-9.96
		25±2/60±2	-9.88	-9.92	-9.97

CONCLUSION

In this study, a modified solvent evaporation method was used to prepare IP-SLN. The release kinetics and permeation characteristics of IP-SLN were investigated, revealing a two-fold increase in permeation compared to ipriflavone (IP). The bone regeneration capacity of IP-SLN was evaluated through ALP activity and calcium mineralization assay. The findings suggest that IP-SLN, as a drug carrier, enhances the bioavailability of ipriflavone and holds the potential for managing osteoporosis. These results highlight the potential of solid lipid nanoparticles as an effective delivery system for improving the therapeutic outcomes of ipriflavone in osteoporosis treatment.

DATA AVAILABILITY

Data will be made available on request

AUTHORS CONTRIBUTIONS

Anish John-Idea generation, work execution, supervision, writing, data compilation, editing, review, submission, Anoop Narayanan V-Idea generation, supervision, editing, review, Sumukh P R-work execution, data compilation, writing, editing, Sneh Priya-Formulation optimization, editing, Chaithra Raviraj-Pharmacokinetic studies, editing, Harsh Ashtekar – Cell-line studies, Pharmacokinetic Studies, editing

CONFLICT OF INTERESTS

The authors declare that there are no conflict of interest regarding the publication of this paper.

REFERENCES

1. Martini M, Formigli L, Tonelli P, Giannelli M, Amunni F, Naldi D. Effects of ipriflavone on perialveolar bone formation. Calcif Tissue Int. 1998 Oct;63(4):312-9. doi: 10.1007/s002239900533, PMID 9744990.
2. Bonucci E, Ballanti P, Martelli A, Mereto E, Brambilla G, Bianco P. Ipriflavone inhibits osteoclast differentiation in parathyroid transplanted parietal bone of rats. Calcif Tissue Int. 1992 Apr;50(4):314-9. doi: 10.1007/BF00301628, PMID 1571842.
3. John A, V AN, Konkodi K. Revisiting ipriflavone: a potential isoflavone for the management of postmenopausal osteoporosis. Rev Bras Farmacogn. 2021 Dec 1;31(6):733-40. doi: 10.1007/s43450-021-00192-z.
4. Dudhani AR, Kosaraju SL. Bioadhesive chitosan nanoparticles: preparation and characterization. Carbohydr Polym. 2010 Jun 11;81(2):243-51. doi: 10.1016/j.carbpol.2010.02.026.

5. Bhatia S. Nanoparticles types classification characterization fabrication methods and drug delivery applications. Nat Polym Drug Deliv Syst. 2016 Sep:33-93. doi: 10.1007/978-3-319-41129-3_2.

6. Sarmento B, Martins S, Ferreira D, Souto EB. Oral insulin delivery by means of solid lipid nanoparticles. Int J Nanomedicine. 2007;2(4):743-9. PMID 18203440.

7. Sailaja A Krishna, Amareshwar P, Chakravarty P. Formulation of solid lipid nanoparticles and their applications. CPR. 2011;1(2):197-203.

8. Mirchandani Y, Patravale VB, SB. Solid lipid nanoparticles for hydrophilic drugs. J Control Release. 2021 Jul 10;335:457-64. doi: 10.1016/j.jconrel.2021.05.032, PMID 34048841.

9. Bhatt S, Sharma J, Singh M, Saini V. Solid lipid nanoparticles: a promising technology for delivery of poorly water-soluble drugs. Acta Pharm Sci. 2018;56(3):27-49. doi: 10.23893/1307-2080.APS.05616.

10. Bhalekar M, Upadhaya P, Madgulkar A. Formulation and characterization of solid lipid nanoparticles for an anti-retroviral drug darunavir. Appl Nanosci. 2017 Feb 1;7(1-2):47-57. doi: 10.1007/s13204-017-0547-1.

11. Liu D, Jiang S, Shen H, Qin S, Liu J, Zhang Q. Diclofenac sodium loaded solid lipid nanoparticles prepared by emulsion/solvent evaporation method. J Nanopart Res. 2011 Jun;13(6):2375-86. doi: 10.1007/s11051-010-9998-y.

12. Harsha SN, Aldhubiab BE, Nair AB, Alhaider IA, Attimarad M, Venugopala KN. Nanoparticle formulation by Buchi b-90 nano spray dryer for oral mucoadhesion. Drug Des Devel Ther. 2015 Jan 23;9:273-82. doi: 10.2147/DDDT.S66654, PMID 25670882.

13. Obinu A, Burrai GP, Cavalli R, Galleri G, Migheli R, Antuofermo E. Transmucosal solid lipid nanoparticles to improve genistein absorption via intestinal lymphatic transport. Pharmaceutics. 2021 Feb 1;13(2):1-17. doi: 10.3390/pharmaceutics13020267, PMID 33669306.

14. Shah I, Vyas J. Role of P-GP inhibitors on gut permeation of metformin: an ex-vivo study. Int J Pharm Pharm Sci. 2022 Oct 1;14(10)18-23. doi: 10.22159/ijpps.2022v14i10.45135.

15. Kim SE, Yun YP, Park K, Kim HJ, Lee DW, Kim JW. The effects of functionalized titanium with alendronate and bone morphogenic protein-2 for improving osteoblast activity. Tissue Eng Regen Med. 2013;10(6):353-61. doi: 10.1007/s13770-013-1098-5.

16. Serguienko A, Wang MY, Myklebost O. Real-time vital mineralization detection and quantification during *in vitro* osteoblast differentiation. Biol Proced Online. 2018 Aug 1;20(1):14. doi: 10.1186/s12575-018-0079-4, PMID 30078998.

17. Wei B, Wang W, Liu X, XU C, Wang Y, Wang Z. Gelatin methacrylate hydrogel scaffold carrying resveratrol loaded solid lipid nanoparticles for enhancement of osteogenic differentiation of BMSCs and effective bone regeneration. Regen Biomater. 2021 Aug 9;8(5):rbab044. doi: 10.1093/rb/rbab044, PMID 34394955.

18. WU S, Wang G, LU Z, LI Y, Zhou X, Chen L. Effects of glycerol monostearate and tween 80 on the physical properties and stability of recombined low-fat dairy cream. Dairy Sci Technol. 2016 Mar 1;96(3):377-90. doi: 10.1007/s13594-015-0274-x.

19. Ahmad N, Banala VT, Kushwaha P, Karvande A, Sharma S, Tripathi AK. Quercetin loaded solid lipid nanoparticles improve osteoprotective activity in an ovariectomized rat model: a preventive strategy for post-menopausal osteoporosis. RSC Adv. 2016 Oct 12;6(100):97613-28. doi: 10.1039/C6RA17141A.

20. Kasongo KW, Pardeike J, Muller RH, Walker RB. Selection and characterization of suitable lipid excipients for use in the manufacture of didanosine-loaded solid lipid nanoparticles and nanostructured lipid carriers. J Pharm Sci. 2011;100(12):5185-96. doi: 10.1002/jps.22711, PMID 22020815.

21. Varshosaz J, Ghaffari S, Khoshayand MR, Atyabi F, Azarmi S, Kobarfard F. Development and optimization of solid lipid nanoparticles of amikacin by central composite design. J Liposome Res. 2010 Jun;20(2):97-104. doi: 10.3109/08982100903103904, PMID 19621981.

22. Bhalekar M, Upadhaya P, Madgulkar A. Formulation and characterization of solid lipid nanoparticles for an anti-retroviral drug darunavir. Appl Nanosci. 2017 Feb 1;7(1-2):47-57. doi: 10.1007/s13204-017-0547-1.

23. Subair TK, Mohanan J. Development of nano-based film forming gel for prolonged dermal delivery of luliconazole. Int J Pharm Pharm Sci. 2022 Feb 1:14(2):31-41. doi: 10.22159/ijpps.2022v14i2.43253.

24. El Assal MI, Samual D. Optimization of rivastigmine chitosan nanoparticles for neurodegenerative alzheimers; *in vitro* and ex vivo characterizations. Int J Pharm Pharm Sci. 2022 Jan 1:14(1):17-27. doi: 10.22159/ijpps.2022v14i1.43145.

25. Charumathy A, Ubaidulla U, Sinha P, Rathnam G. Recent update on liposome-based drug delivery system. Int J Curr Pharm Sci. 2022 May 15:14(3):22-7. doi: 10.22159/ijcpr.2022v14i3.1991.

26. Obinu A, Burrai GP, Cavalli R, Galleri G, Migheli R, Antuofermo E. Transmucosal solid lipid nanoparticles to improve genistein absorption via intestinal lymphatic transport. Pharmaceutics. 2021 Feb 16;13(2):267. doi: 10.3390/pharmaceutics13020267, PMID 33669306.

27. SHAH I, VYAS J. Role of P-GP inhibitors on gut permeation of metformin: an ex-vivo study. Int J Pharm Pharm Sci. 2022 Oct 1:14(10):18-23. doi: 10.22159/ijpps.2022v14i10.45135.

28. SHAH I, VYAS J. Role of P-GP inhibitors on gut permeation of metformin: an ex-vivo study. Int J Pharm Pharm Sci. 2022 Oct 1:18-23.

29. Alghazwani Y, Venkatesan K, Prabahar K, El Sherbiny M, Elsherbiny N, Qushawy M. The combined anti-tumor efficacy of bioactive hydroxyapatite nanoparticles loaded with altretamine. Pharmaceutics. 2023 Jan 1;15(1):302. doi: 10.3390/pharmaceutics15010302, PMID 36678930.

30. Kim SE, Yun YP, Park K, Kim HJ, Lee DW, Kim JW. The effects of functionalized titanium with alendronate and bone morphogenic protein-2 for improving osteoblast activity. Tissue Eng Regen Med. 2013 Nov 13;10(6):353-61. doi: 10.1007/s13770-013-1098-5.

31. Kim SE, Yun YP, Park K, Kim HJ, Lee DW, Kim JW. The effects of functionalized titanium with alendronate and bone morphogenic protein-2 for improving osteoblast activity. Tissue Eng Regen Med. 2013 Nov 13;10(6):353-61. doi: 10.1007/s13770-013-1098-5.

32. Serguienko A, Wang MY, Myklebost O. Real-time vital mineralization detection and quantification during *in vitro* osteoblast differentiation. Biol Proced Online. 2018 Aug 1;20(1):14. doi: 10.1186/s12575-018-0079-4, PMID 30078998.

33. Gregory CA, Gunn WG, Peister A, Prockop DJ. An Alizarin Red based assay of mineralization by adherent cells in culture: comparison with cetylpyridinium chloride extraction. Anal Biochem. 2004 Jun 1;329(1):77-84. doi: 10.1016/j.ab.2004.02.002, PMID 15136169.

34. Ravi GS, Charyulu RN, Dubey A, Prabhu P, Hebbar S, Mathias AC. Nano lipid complex of rutin: development characterisation and *in vivo* investigation of hepatoprotective antioxidant activity and bioavailability study in rats. AAPS Pharm Sci Tech. 2018 Nov 1;19(8):3631-49. doi: 10.1208/s12249-018-1195-9, PMID 30280357.

35. Duong VA, Nguyen TT, Maeng HJ. Preparation of solid lipid nanoparticles and nanostructured lipid carriers for drug delivery and the effects of preparation parameters of solvent injection method. Molecules. 2020 Oct 18;25(20):4781. doi: 10.3390/molecules25204781, PMID 33081021.

36. Kumar R, Yasir M, Saraf SA, Gaur PK, Kumar Y, Singh AP. Glyceryl monostearate based nanoparticles of mefenamic acid: fabrication and *in vitro* characterization. Drug Invent Today. 2013 Sep 1;5(3):246-50. doi: 10.1016/j.dit.2013.06.011.

37. WU S, Wang G, LU Z, LI Y, Zhou X, Chen L. Effects of glycerol monostearate and tween 80 on the physical properties and stability of recombined low-fat dairy cream. Dairy Sci Technol. 2016 Mar 1;96(3):377-90. doi: 10.1007/s13594-015-0274-x.

38. Chen X, Wang T. Preparation and characterization of atrazine loaded biodegradable PLGA nanospheres. J Integr Agric. 2019 May 1;18(5):1035-41. doi: 10.1016/S2095-3119(19)62613-4.

39. Helgason T, Awad TS, Kristbergsson K, McClements DJ, Weiss J. Effect of surfactant surface coverage on formation of solid lipid nanoparticles (SLN). J Colloid Interface Sci. 2009 Jun 1;334(1):75-81. doi: 10.1016/j.jcis.2009.03.012, PMID 19380149.

40. Nazarova A, Yakimova L, Filimonova D, Stoikov I. Surfactant effect on the physicochemical characteristics of solid lipid

nanoparticles based on pillar[5]arenes. Int J Mol Sci. 2022 Jan 1;23(2):779. doi: 10.3390/ijms23020779, PMID 35054962.

41. Kato K, Walde P, Koine N, Ichikawa S, Ishikawa T, Nagahama R. Temperature-sensitive nonionic vesicles prepared from span 80 (sorbitan monooleate). Langmuir. 2008 Oct 7;24(19):10762-70. doi: 10.1021/la801581f, PMID 18720959.

42. YU Z, Fan W, Wang L, QI J, LU Y, WU W. Effect of surface charges on oral absorption of intact solid lipid nanoparticles. Mol Pharm. 2019;16(12):5013-24. doi: 10.1021/acs.molpharmaceut.9b00861, PMID 31638827.

43. Harde H, Das M, Jain S. Solid lipid nanoparticles: an oral bioavailability enhancer vehicle. Expert Opin Drug Deliv. 2011 Nov;8(11):1407-24. doi: 10.1517/17425247.2011.604311, PMID 21831007.

44. Xie K, Gao X, Xiao C, Molinari N, Angioletti Uberti S. Rationalizing the effect of shape and size in nanoparticle-based glues. J Phys Chem C. 2022 May 5;126(17):7517-28. doi: 10.1021/acs.jpcc.2c00461.

45. Gavze E, Shapiro M. Particles in a shear flow near a solid wall: effect of nonsphericity on forces and velocities. Int J Multiphase Flow. 1997 Feb 1;23(1):155-82. doi: 10.1016/S0301-9322(96)00054-7.

46. Muro S, Garnacho C, Champion JA, Leferovich J, Gajewski C, Schuchman EH. Control of endothelial targeting and intracellular delivery of therapeutic enzymes by modulating the size and shape of ICAM-1-targeted carriers. Mol Ther. 2008 Aug 1;16(8):1450-8. doi: 10.1038/mt.2008.127, PMID 18560419.

47. Pathak S, Vyas SP, Pandey A. Development characterization and *in vitro* release kinetic studies of ibandronate loaded chitosan nanoparticles for effective management of osteoporosis. Int J App Pharm. 2021 Nov 7;13(6):120-5. doi: 10.22159/ijap.2021v13i6.42697.

48. Reddy G, Sood S. Solid lipid nanoparticles for oral delivery of poorly soluble drugs. J Pharm Sci & Res. 2012;4(7):1848-55.

49. Righeschi C, Bergonzi MC, Isacchi B, Bazzicalupi C, Gratteri P, Bilia AR. Enhanced curcumin permeability by SLN formulation: the PAMPA approach. LWT Food Sci Technol. 2016 Mar 1;66:475-83. doi: 10.1016/j.lwt.2015.11.008.

50. Scioli Montoto S, Muraca G, Ruiz ME. Solid lipid nanoparticles for drug delivery: pharmacological and biopharmaceutical aspects. Front Mol Biosci. 2020 Oct 30;7:587997. doi: 10.3389/fmolb.2020.587997, PMID 33195435.

51. Turksen K, Bhargava U, Moe HK, Aubin JE. Isolation of monoclonal antibodies recognizing rat bone-associated molecules *in vitro* and *in vivo*. J Histochem Cytochem. 1992;40(9):1339-52. doi: 10.1177/40.9.1506671, PMID 1506671.

52. Alcala Orozco CR, Mutreja I, Cui X, Kumar D, Hooper GJ, Lim KS. Design and characterisation of multi-functional strontium gelatin nanocomposite bioinks with improved print fidelity and osteogenic capacity. Bioprinting. 2020 Jun 1;18:e00073. doi: 10.1016/j.bprint.2019.e00073.

53. Van der Horst G, Van Bezooijen RL, Deckers MM, Hoogendam J, Visser A, Lowik CW. Differentiation of murine preosteoblastic KS483 cells depends on autocrine bone morphogenetic protein signaling during all phases of osteoblast formation. Bone. 2002 Dec 1;31(6):661-9. doi: 10.1016/s8756-3282(02)00903-1, PMID 12531559.